

Electronic Structure and Phase Stability of Yb-filled CoSb₃ Skutterudite Thermoelectrics from First Principles

Eric B. Isaacs and Chris Wolverton*

Department of Materials Science and Engineering, Northwestern University, Evanston, Illinois 60208, USA

E-mail: c-wolverton@northwestern.edu

Abstract

Filling the large voids in the crystal structure of the skutterudite CoSb₃ with rattler atoms R provides an avenue for both increasing carrier concentration and disrupting lattice heat transport, leading to impressive thermoelectric performance. While the influence of R on the lattice dynamics of skutterudite materials has been well studied, the phase stability of R -filled skutterudite materials and the influence of the presence and ordering of R on the electronic structure remain unclear. Here, focusing on the Yb-filled skutterudite Yb _{x} Co₄Sb₁₂, we employ first-principles methods to compute the phase stability and electronic structure. Yb-filled CoSb₃ exhibits (1) a mild tendency for phase separation into Yb-rich and Yb-poor regions and (2) a strong tendency for chemical decomposition into Co–Sb and Yb–Sb binaries (i.e., CoSb₃, CoSb₂, and YbSb₂). We find that, at reasonable synthesis temperatures, configurational entropy stabilizes single-phase solid solutions with limited Yb solubility, in agreement with experiments. Filling CoSb₃ with Yb increases the band gap, enhances the carrier effective masses, and generates new low-energy “emergent” conduction band minima, which is distinct from the traditional band convergence picture of aligning the energies of existing band extrema. The explicit presence of R is necessary to achieve the emergent conduction band minima, though the rattler ordering does not

strongly influence the electronic structure. The emergent conduction bands are spatially localized in the Yb-rich regions, unlike the delocalized electronic states at the Brillouin zone center that form the unfilled skutterudite band edges.

Introduction

In thermoelectric heat-to-electricity conversion, the figure of merit is $ZT = \sigma S^2 T / \kappa$, where σ is the electrical conductivity, S is the thermopower, κ is the thermal conductivity, and T is the temperature. Therefore, efficient thermoelectric materials must exhibit a rare combination of electronic and thermal transport properties: large σ , large S , and small κ . In order to (1) understand the ability of existing thermoelectric materials, typically heavily doped semiconductors, to satisfy this set of rare physical properties and (2) design improved thermoelectric materials, a detailed understanding of the electronic structure, lattice dynamics, and phase stability is critically important.

One famous class of thermoelectric materials is the skutterudite CoSb₃, a covalent semiconductor satisfying the 18-electron rule.³ CoSb₃, whose skutterudite crystal structure is shown in Fig. 1, can be considered a perovskite (ABX₃, with an empty A-site) with substantial distortions of the CoSb₆ octahedra that create large voids.¹ CoSb₃ has a body-centered-cubic (bcc)

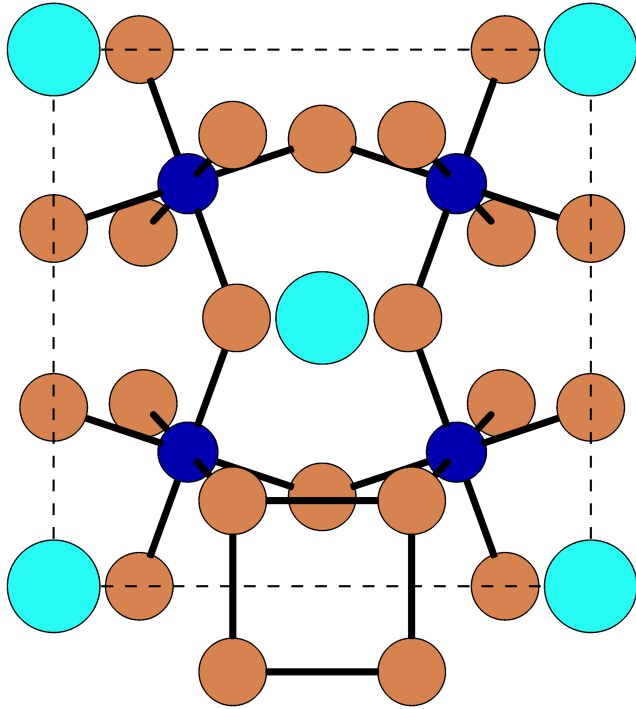


Figure 1: Skutterudite crystal structure. The conventional unit cell is shown with the black dashed lines and cyan, blue, and brown circles indicate Yb/vacancy, Co, and Sb, respectively. We note that there is an alternative crystal structure description in terms of Sb_4 rings (sometimes called squares or rectangles);^{1,2} one such ring is shown.

lattice with 16 atoms in the primitive unit cell and a space group of $Im\bar{3}$. CoSb_3 -based thermoelectric materials exhibit favorable electronic transport properties, as the highly covalent bonding leads to large electronic mobility μ and σ (but also increasing κ_e , the electronic contribution to κ).⁴ In addition, the presence of a high-degeneracy conduction band minimum close in energy to the conduction band minima at the Brillouin zone center has been invoked to rationalize the large S , via the concept of band convergence.^{5,6}

Perhaps the most distinguishing feature of skutterudite materials is their ability to host “rattler” atoms R (such as alkali, alkaline earth, actinide, rare earth, and halogen elements) in the large crystallographic voids,⁷ which serves a dual purpose with respect to thermoelectricity. First, it enhances the power factor (σS^2) via electronic doping.⁸ Secondly, it drastically reduces κ_L , the lattice component of κ .⁹ Loosely bonded to the rest of the solid, the rattler atoms are believed to disrupt phonon transport via “rattling” in the voids (hence the name).^{10–13}

While the influence of rattlers on the lattice dynamical properties of skutterudite materials has been much studied,^{14–38} the phase stability and electronic properties have received far less attention. In particular, the thermodynamic stability of filled skutterudite materials, the ordering tendencies of the rattlers, and the precise influence of the rattlers on the electronic states are all unclear. Therefore, in this work, we present a detailed study of the phase stability and electronic structure of filled skutterudite CoSb_3 using first-principles calculations. We focus on Yb rattlers since Yb-filled skutterudite CoSb_3 exhibits some of the most promising thermoelectric properties, e.g., ZT approaching 1.5, and has been subject to considerable experimental investigation.^{7,39}

We find that the Yb-filled skutterudite exhibits a tendency to phase separate into Yb-rich and Yb-poor regions, though the energetic lowering (compared to the completely empty and filled endmembers) is only on the order of 10 meV per Yb/void site. Due to the small magnitude of the formation energy, configurational entropy will likely win this energetic battle,

consistent with the single-phase solid solutions typically found in experiment. The Yb-filled skutterudite is in a three-phase region of the thermodynamic convex hull, with a substantial thermodynamic driving force for chemical decomposition into binaries. We find that this chemical decomposition tendency limits the Yb solubility, in agreement with experiments. Filling the CoSb_3 skutterudite with Yb opens the electronic band gap, increases the carrier effective masses, and leads to the emergence of several new conduction band minima. The explicit presence, though not the ordering, of the rattlers is responsible for the new conduction band minima, which are not present in the unfilled skutterudite, as would be the case for the traditional band convergence picture. The emergent conduction bands exhibit distinct character with spatial localization in the Yb-rich regions, as compared to the delocalized electronic states at the Brillouin zone center.

Computational Methodology

As can be observed in Fig. 1, CoSb_3 exhibits a significant octahedral distortion ($a^+a^+a^+$ in Glazer notation⁴⁰) with respect to the ideal perovskite structure. While $\angle\text{Co-Sb-Co}$ is 180° for perovskite, it is 127° in CoSb_3 . Similarly, $\angle\text{Sb-Co-Sb}$ is $85-95^\circ$ instead of the ideal 90° . The octahedral distortion in the skutterudite crystal structure yields 1 void per 4 Co atoms. Therefore, the general stoichiometry for a filled CoSb_3 skutterudite is $R_x\text{Co}_4\text{Sb}_{12}$ with $0 < x < 1$. Using \square to explicitly indicate an empty void, the formula becomes $\square_{1-x}R_x\text{Co}_4\text{Sb}_{12}$. We note that the upper limit of x , i.e., the filling fraction limit (FFL), is lower than 1 in practice,⁴¹⁻⁴⁴ but we consider the full crystallographic range of $0 \leq x \leq 1$.

Plane-wave density functional theory (DFT)^{45,46} calculations are performed using VASP⁴⁷ w/ the generalized gradient approximation of Perdew, Burke, and Ernzerhof⁴⁸ using Co, Sb, and Yb_2 ($5p^66s^2$ valence) projector augmented wave (PAW) potentials.^{49,50} We use a 500 eV kinetic energy cutoff, Γ -centered k -point grids of density ≥ 500 k -points/ \AA^{-3} ,

0.1 eV 1st-order Methfessel-Paxton smearing⁵¹ for structural relaxations, and the tetrahedron method with Blöchl corrections⁵² for static runs. The energy and ionic forces are converged to 10^{-6} eV energy and 10^{-2} eV/ \AA , respectively. Given the reaction energy for $\text{Yb} + 2\text{CoSb}_3 \rightarrow \text{YbSb}_2 + 2\text{CoSb}_2$ changes by only 20 meV/Yb (1.3%) via the inclusion of the $4f$ states in the Yb PAW potential, we expect the absence of such states will not significantly affect our results.

The convex hull is constructed from the Open Quantum Materials Database (OQMD),^{53,54} a database of electronic structure calculations based on DFT, which contains 49 binary and 5 ternary phases in the Yb-Co-Sb space (as of June 2018). A cluster expansion (CE)^{55,56} is employed to describe the energetics of different configurations of Yb and \square on the bcc sublattice of voids in the skutterudite structure. The optimal CE in ATAT⁵⁷ contains null, point, and pair (out to 6th nearest neighbor) clusters. Disordered structures are modeled with special quasirandom structures (SQS)⁵⁸ with 8 Yb/ \square sites for x of $1/4$, $1/2$, and $3/4$.⁵⁹ To generate an analytical representation of the x -dependent energetics of SQS, we fit the formation energies of the SQS to a Redlich-Kister polynomials of order 1 (subregular solution model), as discussed in Refs. 60 and 61. Band structure unfolding based on the CoSb_3 lattice parameter is performed using BANDUP.^{62,63}

Results and Discussion

Phase stability

Figure 2(a), which contains the Yb-Co-Sb ternary convex hull based on the OQMD, shows that $\text{Yb}_x\text{Co}_4\text{Sb}_{12}$ is in a 3-phase region of the convex hull bounded by CoSb_3 , CoSb , and $\text{Yb}_{11}\text{Sb}_{10}$. In other words, $\text{Yb}_x\text{Co}_4\text{Sb}_{12} \rightarrow (4 - 5x/11)\text{CoSb}_3 + (5x/11)\text{CoSb} + (x/11)\text{Yb}_{11}\text{Sb}_{10}$ is the lowest-energy decomposition reaction according to the OQMD. Experiments instead suggest the competing phases CoSb_3 , CoSb_2 , and YbSb_2 ,^{42,64} so we focus on the corresponding decomposition reaction. Although CoSb_2

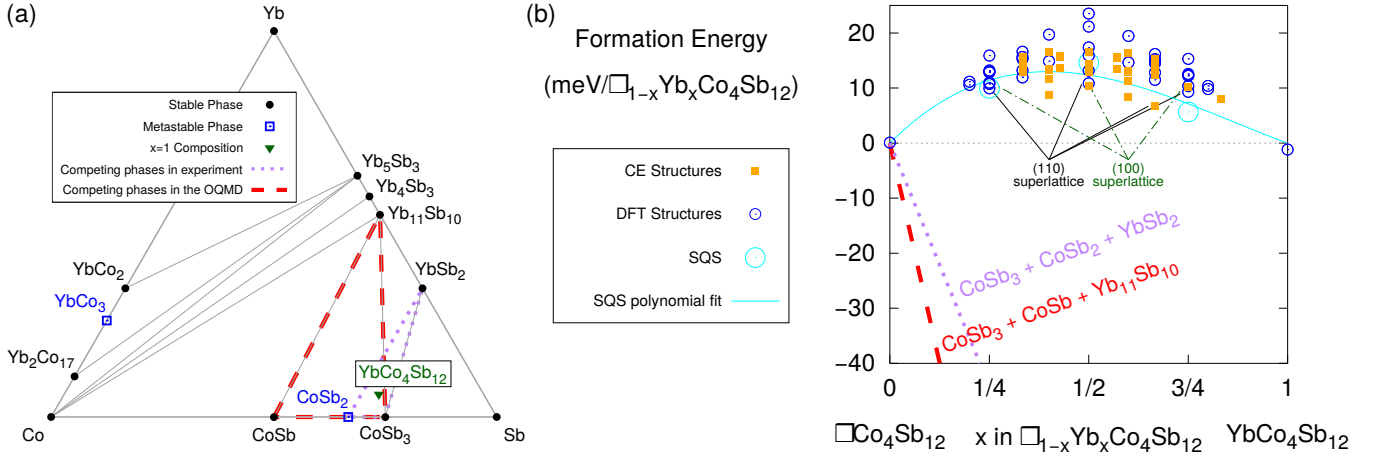


Figure 2: (a) Yb–Co–Sb ternary convex hull from the OQMD. In addition to the stable phases (black filled circles connected by grey tie lines), we indicate two metastable phases (above the hull by 7 meV/atom for YbCo_3 , 4 meV/atom for CoSb_2) with open blue squares. $\text{Yb}_x\text{Co}_4\text{Sb}_{12}$ corresponds to the line (not drawn) between the $\text{YbCo}_4\text{Sb}_{12}$ composition (filled green triangle) and CoSb_3 . The vertices of the red dashed triangle indicates the decomposition products for the lowest-energy decomposition reaction for $\text{Yb}_x\text{Co}_4\text{Sb}_{12}$; those of the smaller purple dotted triangle correspond to an alternate decomposition reaction discussed in the text. (b) Cluster expansion formation energy as a function of Yb concentration for structures used to fit the cluster expansion (open blue circles) and those predicted by the cluster expansion (solid orange squares). The DFT-computed formation energy for SQS (large open cyan circles) and a polynomial fit (cyan line) are also shown. In panel (b), the thick lines in the region of negative formation energy correspond to the formation energy of the two decomposition reactions indicated in panel (a).

is metastable, it is above the convex hull by only 4 meV/atom. Given this small energy, it is conceivable that vibrational entropy (not computed in this work) might stabilize this phase. Artificially lowering the energy of CoSb_2 alone is not sufficient to make $\text{Yb}_x\text{Co}_4\text{Sb}_{12} \rightarrow (4-2x)\text{CoSb}_3 + 2x\text{CoSb}_2 + x\text{YbSb}_2$ the lowest-energy decomposition reaction. However, as discussed in the Supporting Information, its combination with stabilizing YbSb_2 and/or destabilizing $\text{Yb}_{11}\text{Sb}_{10}$ can achieve this effect. For example, the three-phase equilibrium of CoSb_3 , CoSb_2 , and YbSb_2 is achieved by the simultaneous artificial energy lowering of CoSb_2 and YbSb_2 by 20 and 23 meV/atom, respectively. Validation of the convex hull from the OQMD is discussed in the Supporting Information.

The formation energies of $\text{Yb}_x\text{Co}_4\text{Sb}_{12}$, with respect to the $x = 0$ and $x = 1$ endmembers, computed via cluster expansion, are shown in Fig. 2(b). The cluster expansion, which is fit to 40 structures, achieves a leave-one-out cross-validation score of 1.6 meV per lattice site. Additional details on the cluster expansion are contained in the Supporting Information. A mild phase separating tendency is observed, with positive formation energies on the order of tens of meV per lattice site. Phase separation has also been predicted in $\text{La}_x\text{Fe}_4\text{Sb}_{12}$ via coherent potential approximation calculations (in this case with appreciable energy of mixing ~ 0.6 eV),³⁷ whereas a previous cluster expansion for $\text{Ba}_x\text{Co}_4\text{Sb}_{12}$ found several stable ordered phases (formation energy no lower than ~ -90 meV).⁶⁵ Among the ordered phases, we find (110) and (100) superlattices are the lowest-energy structures (still higher in energy than phase separation).

The SQS exhibit DFT-computed formation energies (6–15 meV) similar to the formation energies of the ordered structures, which is reflective of the relatively weak interaction between the rattlers. Therefore, given the small magnitude of the formation energy, we expect configurational entropy to easily overcome the phase separation tendency at reasonable synthesis temperatures and enable single-phase solid solutions of $\text{Yb}_x\text{Co}_4\text{Sb}_{12}$. For example, the ideal configurational entropy contribution

to the mixing free energy, $-k_B T[(1-x)\ln(1-x) + x\ln(x)]$, where k_B is the Boltzmann constant, is ≈ -44 meV for $x = 1/4$ at 900 K, which is significantly larger in magnitude than the mixing energy (≈ 10 meV).

The thermodynamic driving force for chemical decomposition into binaries, on the other hand, is much stronger than the phase separation tendency. As shown by the steep negatively sloped lines in Fig. 2(b), the formation energies for chemical decomposition are significantly larger in magnitude than the mixing energy. For example, the formation energy for the appropriate linear combination of CoSb_3 , CoSb_2 , and YbSb_2 [dotted purple line in Fig. 2(b)] for $x = 1/4$ is ≈ -44 meV. Therefore, the chemical decomposition tendency serves to limit the solubility of Yb in CoSb_3 , as has been suggested by previous theoretical works.^{66–69}

In experiments, a phase of $\text{Yb}_x\text{Co}_4\text{Sb}_{12}$ with a maximum in Yb content is typically achieved without evidence of Yb ordering or separation into Yb-rich and Yb-poor phases; this phase often coexists with the binary impurity phases CoSb_2 and YbSb_2 .^{42,44,70–73} This behavior is qualitatively consistent with our computational findings. We note that samples whose preparation involves ball milling may exhibit an inhomogeneous Yb distribution due to non-equilibrium effects, however.⁷⁴

Although it has received considerable attention in the literature, the solubility (FFL) of Yb in CoSb_3 remains controversial, with values reported ranging from 0.2 to 0.7.^{41–43,66,73,75} Here, we address this important issue by computing the solubility from our first-principles calculations and comparing directly to past theoretical calculations and recent experiments. In our work, we take a subregular solid solution model (corresponding to the polynomial fit to SQS energetics discussed above) and quantitatively incorporate ideal configurational entropy; vibrational entropy is discussed below. To compute the solubility, we employ the common tangent construction with respect to the binary decomposition products observed in experiment (CoSb_2 and YbSb_2). Further details on the evaluation of the solubility from our calculations, as well as details on the comparison data

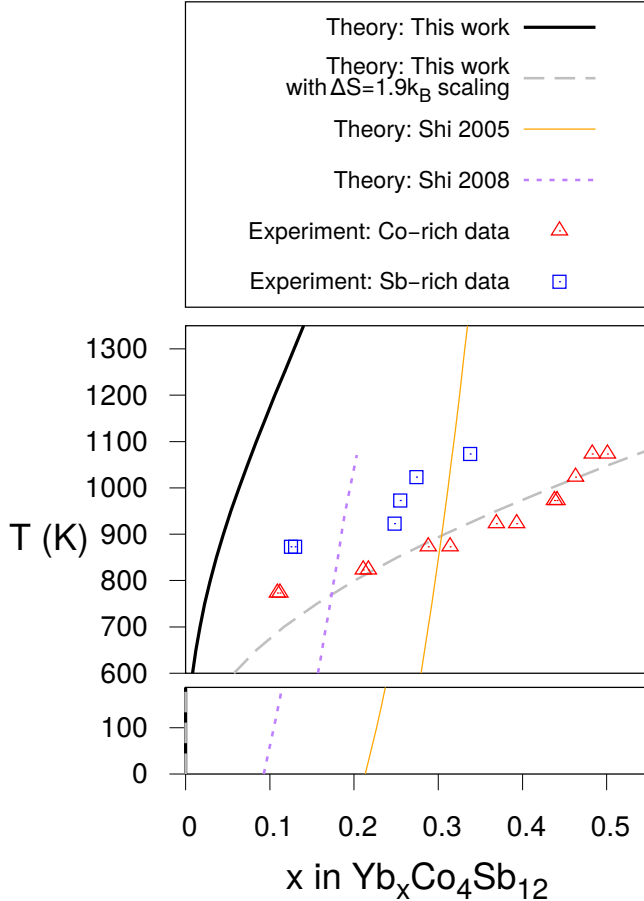


Figure 3: Temperature-dependent solubility (filling fraction limit) of $\text{Yb}_x\text{Co}_4\text{Sb}_{12}$. The computed solvus from this work is shown without (thick solid black line) and with (dashed grey line) the scaling factor $e^{\Delta S/k_B}$ for a vibrational entropy change $\Delta S = 1.9 k_B$, as discussed in the main text. Past theoretical solubility predictions from Refs. 66 (thin solid orange line, labeled Shi 2005) and 69 (thin dashed purple line, labeled Shi 2008) are included for comparison. Experimental data for the Co-rich (red open triangles) and Sb-rich (blue open squares) region of the experimental phase diagram are taken from Fig. 4 of Ref. 42.

from past theoretical studies, are included in the Supporting Information.

Figure 3 illustrates our computed (thick solid black line) temperature-dependent solubility curve (solvus) for Yb in CoSb_3 in comparison with past theory and experiments. The previous theoretical calculations of Refs. 66 (thin solid orange line) and 69 (thin dashed purple line) found relatively small temperature dependence. In addition, the similar previous theoretical work of Mei *et al.* reported a single FFL value (0.30) rather than temperature-dependent results.⁶⁷ The lack of strong temperature dependence in the past theoretical works is in disagreement with the experimental results of Tang *et al.*, who observed the measured solubility can vary by as much as a factor of five as a function of annealing temperature.⁴² Importantly, the past theory works also found finite solubility for $T \rightarrow 0$. Since entropy must vanish for $T \rightarrow 0$ (third law of thermodynamics), such a solid solution cannot exist on the $T = 0$ phase diagram.⁷⁶ In this sense, the past theoretical predictions violate the third law. They also are inconsistent with experiments, which suggest FFL approaching 0 for $T \rightarrow 0$.⁴² We note that it may be possible to maintain a finite rattler concentration at low T in experiment, but only as a result of kinetic effects.

In contrast to the past theoretical works, we correctly find a vanishing solubility at low temperature, which is consistent with the third law and agrees with experiment.⁴² Figure 3 shows a quantitative comparison of our computed solvus with experimental data from Ref. 42 for the solubility in the Co-rich (red open triangles) and Sb-rich (blue open squares) regions of the experimental phase diagram. We focus on the Co-rich data since it corresponds to equilibrium of $\text{Yb}_x\text{Co}_4\text{Sb}_{12}$ with CoSb_2 and YbSb_2 .⁴² Our computed values appreciably underestimate the experimental solubility. As a result, although we find a larger temperature dependence compared to past theoretical works (and the correct exponential dependence in the dilute limit), our computed temperature dependence is still significantly smaller than experiment.⁴² This solubility underestimation has been commonly observed in first-principles pre-

dictions due to the neglect of vibrational entropy.^{77–80} Given Yb is a rattler, corresponding to low-frequency vibrational modes, one can expect the inclusion of vibrational entropy to significantly stabilize the $\text{Yb}_x\text{Co}_4\text{Sb}_{12}$ solid solution, enhancing the solubility. Via fitting, we find that a vibrational formation entropy ΔS (of the solid solution with respect to the linear combination of binary decomposition products) of $1.9 k_B$, taken to modify the solubility via a $e^{\Delta S/k_B}$ multiplicative factor (dilute limit approximation), is sufficient to reconcile the theoretical prediction with experiment, as shown in Fig. 3. Experimental measurements and/or calculations of the phonon entropy will be important future work towards achieving quantitative solubility prediction for skutterudite materials. We note that, beyond vibrational entropy, non-ideal configurational entropy may also help reconcile the computational results with experiment.

Endmember electronic band structure

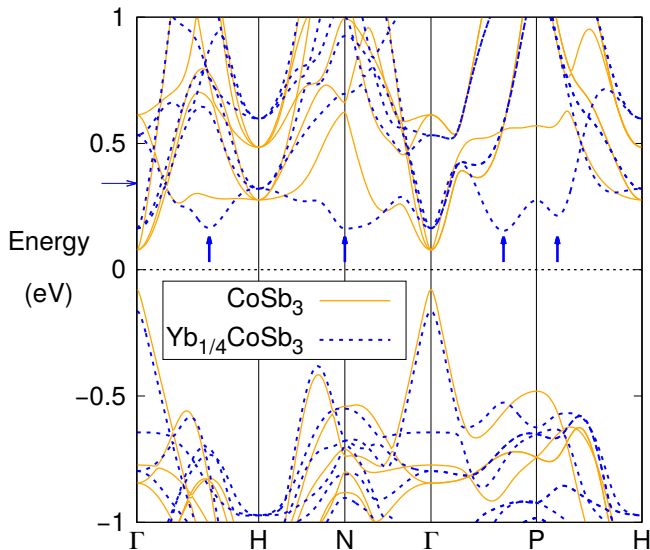


Figure 4: Electronic band structure of $\text{Yb}_x\text{Co}_4\text{Sb}_{12}$ for the fully-relaxed endmembers ($x = 0$ and $x = 1$). Energies are plotted with respect to the gap midpoint at Γ , and the Fermi energy for $x = 1$ is indicated by the horizontal arrow. Emergent conduction band minima in $x = 1$ are noted by the vertical arrows.

The electronic band structure of the endmembers ($x = 0$ and $x = 1$) is shown in Fig. 4. Filling the voids with Yb ($x > 0$) leads to a metallic state with carriers in the conduction band. For comparison, the zero of energy set to gap midpoint at Γ . Here, both the $x = 0$ and $x = 1$ structures are fully relaxed, so $x = 1$ has a smaller Brillouin zone volume than that of $x = 0$ due to a larger lattice parameter. We note that we find the same trends discussed below if we fix to the relaxed $x = 0$ lattice parameter.

With Co contributing $9 e^-$ and Sb_3 contributing $9 e^-$, CoSb_3 satisfies the $18 e^-$ rule³ and forms a semiconductor with a small experimental band gap on the order of 35–50 meV.^{81,82} We find CoSb_3 is a direct-gap semiconductor, with the singly-degenerate valence band and triply-degenerate conduction bands located at Γ , consistent with previous calculations.^{5,83,84} The valence bands are primarily a mix of Co p/d and Sb p character, whereas the conduction bands are primarily Co d character. As shown in early electronic structure calculations on CoSb_3 ,^{83,84} the valence band and one of the conduction bands exhibit linear dispersion (as opposed to the usual parabolic behavior) near the band extrema.

Filling the voids of CoSb_3 with Yb leads to two major effects. First of all, it can be seen that adding Yb increases the magnitude of the band gap. Secondly, the Yb rattlers lead to the emergence of additional conduction band minima close in energy to the band edge at Γ . We observe such bands, which we refer to as “emergent bands” for reasons discussed in the next section, at four locations along the high-symmetry k -path shown in Fig. 4: (1) between Γ and H, (2) at N, (3) between P and Γ , and (4) between P and H. We note that another emergent band minima exists between N and H, not shown in Fig. 4. For sufficiently large x , the conduction band minimum no longer corresponds to the band at Γ , i.e., the direct gap at Γ is no longer the smallest gap. The same trends of band gap opening and new, emergent conduction band minima are also present for intermediate x values, as discussed below.

Here, we discuss the band gap trends in more

detail. Although semilocal DFT is well known to exhibit errors in band gaps,⁸⁵ quasiparticle and spin-orbit coupling corrections have been shown to yield only small changes to the gap (~ 0.1 eV) in this system,^{86,87} and we expect the computed trends to be valid even if there are small errors in the absolute values. The computed band gap of CoSb₃, 0.155 eV, is larger but still comparable to the small experimental band gap on the order of 35–50 meV.^{81,82} Fully filling the voids with Yb (corresponding to the $x = 1$ structure) increases the gap to 0.210 eV. The band gap increases further to 0.239 eV if we fix to CoSb₃ structural parameters; this indicates the gap opening is a chemical, not structural, effect. In order to understand the role of the Yb atoms, we also artificially dope CoSb₃ by increasing the electron chemical potential of CoSb₃ and adding compensating homogeneous background charge to retain charge neutrality, rather than including Yb atoms. In such artificially doped CoSb₃, we find a substantial band gap of 0.315 eV, which indicates that gap opening upon doping is not specifically tied to the presence of Yb as the rattler. Similar behavior was found in a previous study of Ba-filled skutterudite CoSb₃,⁸⁸ which suggests the effect is largely invariant to the nature of the rattler. In contrast to the band gap opening behavior, the emergence of new, low-energy conduction band minima is *not* found for the artificially-doped $x = 1$ case, whose band structure is shown in the Supporting Information. This indicates that the presence of the rattler atoms is responsible for the emergent conduction band minima.

Filling the voids with Yb also impacts the carrier effective masses m^* determined via a quadratic fit of the band structure near the band extrema. The effective masses become larger (corresponding to less dispersive bands) for $x = 1$ as compared to $x = 0$. For example, for the valence band at Γ along the P direction, the effective mass is $0.06 m_e$ for $x = 0$ as compared to $0.09 m_e$ for $x = 1$. Along this direction, there are two heavy and one light conduction band. For $x = 0$, the corresponding effective masses are $0.19 m_e$ and $0.07 m_e$, appreciably smaller than the $0.21 m_e$ and $0.11 m_e$ for $x = 1$, respectively. The same qualitative trend

is found for the Γ valence and conduction bands along each of the k -space directions along the computed high-symmetry path in the Brillouin zone, as is discussed in the Supporting Information. The decrease in carrier mobility ($\sim 1/m^*$) for larger x is consistent with experiments.⁷⁴

Electronic structure of partially-filled skutterudite CoSb₃

In order to probe the electronic properties of Yb _{x} Co₄Sb₁₂ with intermediate x ($0 < x < 1$), we compute the effective band structures for structures with partial Yb filling, as shown in Fig. 5. For ordered structures, we choose the low-energy structures corresponding to (110) superlattices since such structures have a relatively small primitive unit cell. In addition, we note that previous DFT calculations found that (110) is the lowest-energy surface.⁸⁹ We compare to disordered structures in order to assess the effect of Yb ordering on the electronic structure. Both the ordered and disordered structures show similar effects as the fully-filled skutterudite material: band gap opening and emergent conduction band minima. This suggests rattler ordering does not have a dramatic effect on the band structure, though the presence of the rattler atoms is necessary to achieve the new conduction band minima (as discussed above). We note that there are differences between the ordered and disordered structures in the finer details of the emergent bands.

In order to investigate the nature of the electronic states in the partially-filled skutterudite material, we compute for the superlattice structures the projections of the wavefunctions (1) on all atoms corresponding to the Yb-rich region (which we call $p_{\text{Yb-rich}}$) and (2) on all atoms corresponding to the Yb-poor region (which we call $p_{\text{Yb-poor}}$). The layers of atoms at the interfaces between these regions are not included in either of these projections. For example, for $x = 1/2$, these interface atoms include those lying in the purple planes drawn in Fig. 5(d) as well as the corresponding atoms between layers 2 and 3. We define the *spatial polarization*, with respect to the Yb-rich and

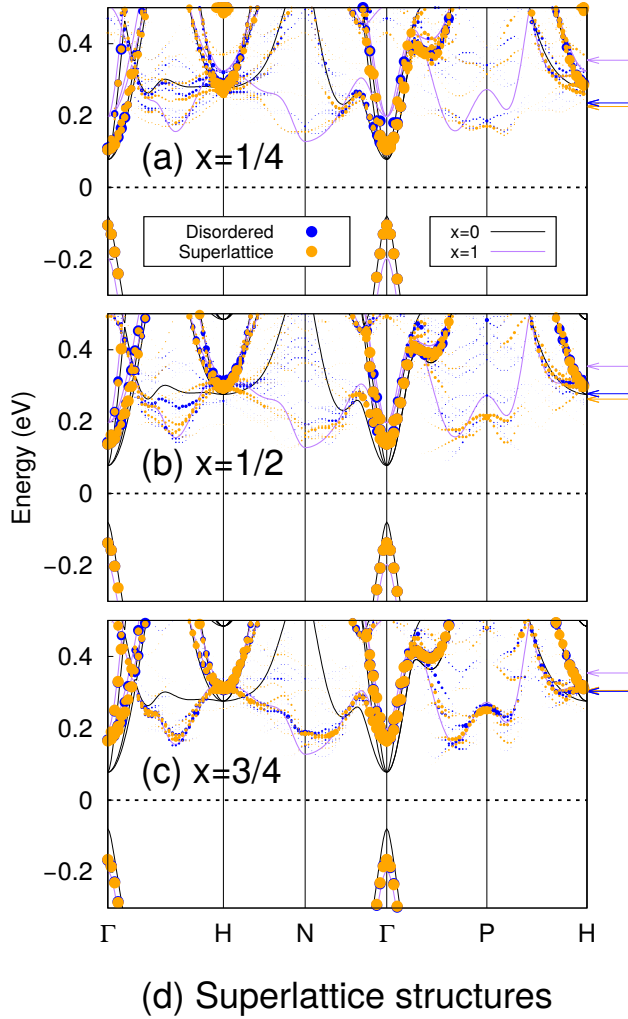


Figure 5: Electronic band structure of the ordered (110) superlattice and disordered structure of $\text{Yb}_x\text{Co}_4\text{Sb}_{12}$ for (a) $x = 1/4$, (b) $x = 1/2$, and (c) $x = 3/4$. Size of the points is proportional to the weight in the effective band structure as determined by band unfolding. For visual clarity, we only plot points with weight greater than 0.02. Fermi energies are indicated by horizontal arrows. The endmember band structures are shown as solid lines. All structures are fixed to the relaxed $x = 0$ lattice parameter. The superlattice structures correspond to retaining Yb in layer 1 for $x = 1/4$, layers 1 and 2 for $x = 1/2$, and layers 1, 2, and 3 for $x = 3/4$ as shown in panel (d).

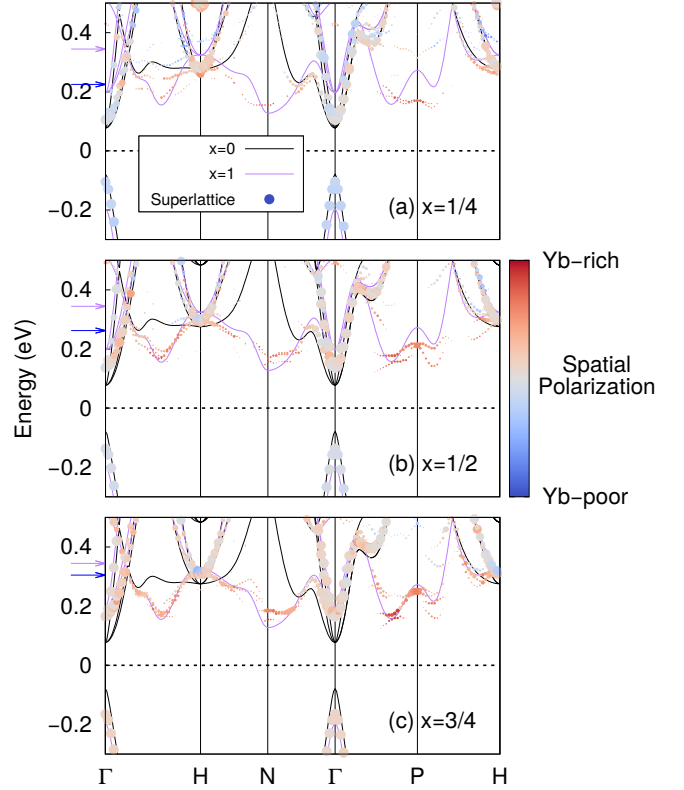


Figure 6: Electronic band structure of the ordered (110) superlattice of $\text{Yb}_x\text{Co}_4\text{Sb}_{12}$ for (a) $x = 1/4$, (b) $x = 1/2$, and (c) $x = 3/4$. Size of the points is proportional to the weight in the effective band structure as determined by band unfolding, and the color indicates the spatial polarization ξ of the wavefunctions (as defined in the main text). We only plot points with weight greater than 0.02 (for visual clarity) whose $p_{\text{Yb-rich}}$ and $p_{\text{Yb-poor}}$ are both greater than 0.025 (to avoid numerical errors in computing ξ). Fermi energies are indicated by horizontal arrows. The endmember band structures are shown as solid lines. All structures are fixed to the relaxed $x = 0$ lattice parameter.

Yb-poor regions, of the electronic states as

$$\xi = \frac{p_{\text{Yb-rich}}/x}{p_{\text{Yb-rich}}/x + p_{\text{Yb-poor}}/(1-x)}.$$

The factors of $1/x$ and $1/(1-x)$ are included to normalize for the differing sizes of the Yb-rich and Yb-poor regions when $x \neq 1/2$. A spatial polarization value of $1/2$ indicates the wavefunction exhibits an equal preference for localization on an atom in the Yb-rich region as that in the Yb-poor region, whereas a ξ value of 1 (0) indicates a 100% preference for localization on an atom in the Yb-rich (Yb-poor) region.

The spatial polarization of the superlattice electronic states is shown via the color of the points in Fig. 6, which shows the superlattice band structure. The emergent conduction bands exhibit values of ξ significantly larger than $1/2$, which indicates such states tend to be localized in the Yb-rich region. Although these states have a strong preference to localize in the Yb-rich *region*, we note that the states are not localized on the Yb atoms, which act as cations and donate their charge. In contrast to the emergent bands, the electronic states at Γ show values of ξ much closer to $1/2$. This indicates that the highly-dispersive bands at Γ are much more spatially delocalized. Therefore, one can think of $\text{Yb}_x\text{Co}_4\text{Sb}_{12}$ as containing two distinct types of carriers: delocalized electrons at Γ and electrons more localized in the Yb-rich regions from the emergent bands.

Finally, we discuss our use of the term “emergent bands” and put our results in the context of the concept of band convergence. The behavior we find is quite distinct from typical band convergence (such as in $\text{PbTe}_{1-x}\text{Se}_x$,⁹⁰ $\text{Mg}_2\text{Si}_{1-x}\text{Sn}_x$,⁹¹ $\text{Pb}_{1-x}\text{Mg}_x\text{Te}$,⁹² and $\text{Pb}_{1-x}\text{Sr}_x\text{Se}$ ⁹³) in which the energies of multiple existing band minima converge as a function of some tuning parameter, such as temperature or doping. In our case, several of the low-energy minima away from Γ are not in general even present (in any recognizable form) in the unfilled material.

For example, as can be seen in Fig. 4 between Γ and P, the lowest-energy conduction band

minimum for $x = 1$ ($\sim 2/3$ of the way from Γ to P), which is associated with the lowest-energy minima along this high-symmetry line in k -space for fractional x in Figs. 5(a-c), essentially does not exist for $x = 0$. In other words, this band minima does not appear at all similar to the band from which it appears to originate, which is the very flat (away from Γ) $x = 0$ band at energy of ~ 0.5 eV in Fig. 4. In this sense, such bands “emerge” rather than “converge” with Yb filling and we describe the new band minima as “emergent bands” rather than “convergent bands.”

The band convergence previously discussed in the literature for skutterudites^{5,6,94} takes a different form than that identified in our work. Since in these previous works the term was applied to the convergence of the energy of an existing conduction band minimum between Γ and N for $x = 0$ (i.e., the lowest-energy minimum roughly halfway from Γ to N in Fig. 4) to that of the conduction band minima at Γ , this corresponds to the typical use of the band convergence term, as discussed above. Our results strongly suggest that several other band minima, including those emergent bands absent in the unfilled material, should also substantially contribute to the electronic transport. Indeed, as shown in Fig. 5(a), even for the lowest filling value considered of $x = 1/4$, these other band minima are significantly lower in energy than the band minimum previously considered in the literature.

Conclusions

Using first-principles calculations, we provide a detailed understanding of the phase stability and electronic properties of filled skutterudite CoSb_3 . The Yb-filled skutterudite $\text{Yb}_x\text{Co}_4\text{Sb}_{12}$ exhibits a mild tendency to phase separate into the Yb-rich and Yb-poor endmembers, as well as a strong tendency for chemical decomposition into Co–Sb and Yb–Sb binaries. Single-phase solid solutions with a limited Yb solubility, observed in experiment, are stabilized by configurational entropy. In addition to enhancing the band gap and effective masses, the pres-

ence of Yb leads to two distinct types of electronic carriers: (1) new emergent conduction band minima whose electronic states are localized near the rattler atoms and (2) the delocalized electronic states at the Brillouin zone center.

Acknowledgement We thank Jeff Snyder (Northwestern) and Wenjie Li (Penn State) for useful discussions. We acknowledge support from the U.S. Department of Energy under Contract de-sc0014520. Computational resources were provided by the National Energy Research Scientific Computing Center (U.S. Department of Energy Contract DE-AC02-05CH11231), the Extreme Science and Engineering Discovery Environment (National Science Foundation Contract ACI-1548562), and the Quest high performance computing facility at Northwestern University.

Supporting Information Available

The following files are available free of charge. Additional details on the Yb–Co–Sb convex hull, $\text{Yb}_x\text{Co}_4\text{Sb}_{12}$ cluster expansion, polynomial fit to formation energies of SQS, computation of solvus and comparison to past solubility predictions, the electronic band structure of artificially doped CoSb_3 , and the carrier effective masses for CoSb_3 and $\text{YbCo}_4\text{Sb}_{12}$.

References

- (1) Schmidt, T.; Kliche, G.; Lutz, H. D. Structure refinement of skutterudite-type cobalt triantimonide, CoSb_3 . *Acta Crystallogr. C* **1987**, *43*, 1678–1679.
- (2) Lefebvre-Devos, I.; Lassalle, M.; Walart, X.; Olivier-Fourcade, J.; Monconduit, L.; Jumas, J. C. Bonding in skutterudites: Combined experimental and theoretical characterization of CoSb_3 . *Phys. Rev. B* **2001**, *63*, 125110.
- (3) Langmuir, I. Types of Valence. *Science* **1921**, *54*, 59–67.
- (4) Snyder, G. J.; Toberer, E. S. Complex thermoelectric materials. *Nat. Mater.* **2008**, *7*, 105–114.
- (5) Tang, Y.; Gibbs, Z. M.; Agapito, L. A.; Li, G.; Kim, H.-S.; Nardelli, M. B.; Curtarolo, S.; Snyder, G. J. Convergence of multi-valley bands as the electronic origin of high thermoelectric performance in CoSb_3 skutterudites. *Nat. Mater.* **2015**, *14*, 1223–1228.
- (6) Hanus, R.; Guo, X.; Tang, Y.; Li, G.; Snyder, G. J.; Zeier, W. G. A Chemical Understanding of the Band Convergence in Thermoelectric CoSb_3 Skutterudites: Influence of Electron Population, Local Thermal Expansion, and Bonding Interactions. *Chem. Mater.* **2017**, *29*, 1156–1164.
- (7) Rogl, G.; Rogl, P. Skutterudites, a most promising group of thermoelectric materials. *Curr. Opin. Green Sust. Chem.* **2017**, *4*, 50–57.
- (8) Nolas, G. S.; Kaeser, M.; Littleton, R. T.; Tritt, T. M. High figure of merit in partially filled ytterbium skutterudite materials. *Appl. Phys. Lett.* **2000**, *77*, 1855–1857.
- (9) Sales, B. C.; Mandrus, D.; Williams, R. K. Filled Skutterudite Antimonides: A New Class of Thermoelectric Materials. *Science* **1996**, *272*, 1325–1328.
- (10) Slack, G. A.; Tsoukala, V. G. Some properties of semiconducting IrSb_3 . *J. Appl. Phys.* **1994**, *76*, 1665–1671.
- (11) Nolas, G. S.; Slack, G. A.; Morelli, D. T.; Tritt, T. M.; Ehrlich, A. C. The effect of rare-earth filling on the lattice thermal conductivity of skutterudites. *J. Appl. Phys.* **1996**, *79*, 4002–4008.
- (12) Nolas, G. S.; Cohn, J. L.; Slack, G. A.; Schujman, S. B. Semiconducting Ge clathrates: Promising candidates for thermoelectric applications. *Appl. Phys. Lett.* **1998**, *73*, 178–180.

- (13) Toberer, E. S.; Zevalkink, A.; Snyder, G. J. Phonon engineering through crystal chemistry. *J. Mater. Chem.* **2011**, *21*, 15843–15852.
- (14) Feldman, J. L.; Singh, D. J.; Mazin, I. I.; Mandrus, D.; Sales, B. C. Lattice dynamics and reduced thermal conductivity of filled skutterudites. *Phys. Rev. B* **2000**, *61*, R9209–R9212.
- (15) Hermann, R. P.; Jin, R.; Schweika, W.; Grandjean, F.; Mandrus, D.; Sales, B. C.; Long, G. J. Einstein Oscillators in Thallium Filled Antimony Skutterudites. *Phys. Rev. Lett.* **2003**, *90*, 135505.
- (16) Feldman, J. L.; Singh, D. J.; Kendziora, C.; Mandrus, D.; Sales, B. C. Lattice dynamics of filled skutterudites: $\text{La}(\text{Fe},\text{Co})_4\text{Sb}_{12}$. *Phys. Rev. B* **2003**, *68*, 094301.
- (17) Viennois, R.; Girard, L.; Koza, M. M.; Mutka, H.; Ravot, D.; Terki, F.; Charar, S.; Tedenac, J.-C. Experimental determination of the phonon density of states in filled skutterudites: evidence for a localized mode of the filling atom. *Phys. Chem. Chem. Phys.* **2005**, *7*, 1617–1619.
- (18) Long, G. J.; Hermann, R. P.; Grandjean, F.; Alp, E. E.; Sturhahn, W.; Johnson, C. E.; Brown, D. E.; Leupold, O.; Ruffer, R. Strongly decoupled europium and iron vibrational modes in filled skutterudites. *Phys. Rev. B* **2005**, *71*, 140302.
- (19) Nolas, G. S.; Fowler, G.; Yang, J. Assessing the role of filler atoms on the thermal conductivity of filled skutterudites. *J. Appl. Phys.* **2006**, *100*, 043705.
- (20) Feldman, J. L.; Dai, P.; Enck, T.; Sales, B. C.; Mandrus, D.; Singh, D. J. Lattice vibrations in $\text{La}(\text{Ce})\text{Fe}_4\text{Sb}_{12}$ and CoSb_3 : Inelastic neutron scattering and theory. *Phys. Rev. B* **2006**, *73*, 014306.
- (21) Wille, H.-C.; Hermann, R. P.; Sergueev, I.; Leupold, O.; van der Linden, P.; Sales, B. C.; Grandjean, F.; Long, G. J.; Ruffer, R.; Shvyd'ko, Y. V. Antimony vibrations in skutterudites probed by ^{121}Sb nuclear inelastic scattering. *Phys. Rev. B* **2007**, *76*, 140301.
- (22) Koza, M. M.; Johnson, M. R.; Viennois, R.; Mutka, H.; Girard, L.; Ravot, D. Breakdown of phonon glass paradigm in La- and Ce-filled $\text{Fe}_4\text{Sb}_{12}$ skutterudites. *Nat. Mater.* **2008**, *7*, 805–810.
- (23) Wang, Y.; Xu, X.; Yang, J. Resonant Oscillation of Misch-Metal Atoms in Filled Skutterudites. *Phys. Rev. Lett.* **2009**, *102*, 175508.
- (24) Dimitrov, I. K.; Manley, M. E.; Shapiro, S. M.; Yang, J.; Zhang, W.; Chen, L. D.; Jie, Q.; Ehlers, G.; Podlesnyak, A.; Camacho, J.; Li, Q. Einstein modes in the phonon density of states of the single-filled skutterudite $\text{Yb}_{0.2}\text{Co}_4\text{Sb}_{12}$. *Phys. Rev. B* **2010**, *82*, 174301.
- (25) Bernstein, N.; Feldman, J. L.; Singh, D. J. Calculations of dynamical properties of skutterudites: Thermal conductivity, thermal expansivity, and atomic mean-square displacement. *Phys. Rev. B* **2010**, *81*, 134301.
- (26) Koza, M. M.; Capogna, L.; Leithe-Jasper, A.; Rosner, H.; Schnelle, W.; Mutka, H.; Johnson, M. R.; Ritter, C.; Grin, Y. Vibrational dynamics of filled skutterudites $M_{1-x}\text{Fe}_4\text{Sb}_{12}$ ($M = \text{Ca}, \text{Sr}, \text{Ba}, \text{and Yb}$). *Phys. Rev. B* **2010**, *81*, 174302.
- (27) Huang, B.; Kaviani, M. Filler-reduced phonon conductivity of thermoelectric skutterudites: Ab initio calculations and molecular dynamics simulations. *Acta Mater.* **2010**, *58*, 4516–4526.
- (28) Möchel, A.; Sergueev, I.; Wille, H.-C.; Voigt, J.; Prager, M.; Stone, M. B.; Sales, B. C.; Guguchia, Z.; Shengelaya, A.; Keppens, V.; Hermann, R. P. Lattice dynamics and anomalous softening in the

- YbFe₄Sb₁₂ skutterudite. *Phys. Rev. B* **2011**, *84*, 184306.
- (29) Wee, D.; Kozinsky, B.; Fornari, M. Frequency of Filler Vibrations in CoSb₃ Skutterudites: A Mechanical Interpretation. *J. Phys. Soc. Jpn.* **2012**, *82*, 014602.
- (30) Zebajjadi, M.; Yang, J.; Lukas, K.; Kozinsky, B.; Yu, B.; Dresselhaus, M. S.; Opeil, C.; Ren, Z.; Chen, G. Role of phonon dispersion in studying phonon mean free paths in skutterudites. *J. Appl. Phys.* **2012**, *112*, 044305.
- (31) Li, W.; Mingo, N. Thermal conductivity of fully filled skutterudites: Role of the filler. *Phys. Rev. B* **2014**, *89*, 184304.
- (32) Feldman, J. L.; Singh, D. J.; Bernstein, N. Lattice-dynamical model for the filled skutterudite LaFe₄Sb₁₂: Harmonic and anharmonic couplings. *Phys. Rev. B* **2014**, *89*, 224304.
- (33) Koza, M. M.; Leithe-Jasper, A.; Rosner, H.; Schnelle, W.; Mutka, H.; Johnson, M. R.; Grin, Y. Vibrational dynamics of the filled skutterudite Yb_{1-x}Fe₄Sb₁₂: Debye-Waller factor, generalized density of states, and elastic structure factor. *Phys. Rev. B* **2014**, *89*, 014302.
- (34) Li, W.; Mingo, N. Ultralow lattice thermal conductivity of the fully filled skutterudite YbFe₄Sb₁₂ due to the flat avoided-crossing filler modes. *Phys. Rev. B* **2015**, *91*, 144304.
- (35) Koza, M. M.; Boehm, M.; Sischka, E.; Schnelle, W.; Mutka, H.; Leithe-Jasper, A. Low-energy phonon dispersion in LaFe₄Sb₁₂. *Phys. Rev. B* **2015**, *91*, 014305.
- (36) Sergueev, I.; Glazyrin, K.; Kantor, I.; McGuire, M. A.; Chumakov, A. I.; Klobes, B.; Sales, B. C.; Hermann, R. P. Quenching rattling modes in skutterudites with pressure. *Phys. Rev. B* **2015**, *91*, 224304.
- (37) Ren, W.; Geng, H.; Zhang, Z.; Zhang, L. Filling-Fraction Fluctuation Leading to Glasslike Ultralow Thermal Conductivity in Caged Skutterudites. *Phys. Rev. Lett.* **2017**, *118*, 245901.
- (38) Fu, Y.; He, X.; Zhang, L.; Singh, D. J. Collective-Goldstone-mode-induced ultralow lattice thermal conductivity in Sn-filled skutterudite SnFe₄Sb₁₂. *Phys. Rev. B* **2018**, *97*, 024301.
- (39) Rull-Bravo, M.; Moure, A.; Fernández, J. F.; Martín-González, M. Skutterudites as thermoelectric materials: revisited. *RSC Adv.* **2015**, *5*, 41653–41667.
- (40) Glazer, A. M. The classification of tilted octahedra in perovskites. *Acta Crystallogr. B* **1972**, *28*, 3384–3392.
- (41) Yang, J.; Hao, Q.; Wang, H.; Lan, Y. C.; He, Q. Y.; Minnich, A.; Wang, D. Z.; Harriman, J. A.; Varki, V. M.; Dresselhaus, M. S.; Chen, G.; Ren, Z. F. Solubility study of Yb in *n*-type skutterudites Yb_xCo₄Sb₁₂ and their enhanced thermoelectric properties. *Phys. Rev. B* **2009**, *80*, 115329.
- (42) Tang, Y.; Chen, S.-w.; Snyder, G. J. Temperature dependent solubility of Yb in Yb–CoSb₃ skutterudite and its effect on preparation, optimization and lifetime of thermoelectrics. *J. Materiomics* **2015**, *1*, 75–84.
- (43) Wang, S.; Salvador, J. R.; Yang, J.; Wei, P.; Duan, B.; Yang, J. High-performance *n*-type Yb_xCo₄Sb₁₂: from partially filled skutterudites towards composite thermoelectrics. *NPG Asia Mater.* **2016**, *8*, e285.
- (44) Ryll, B.; Schmitz, A.; de Boor, J.; Franz, A.; Whitfield, P. S.; Reehuis, M.; Hoser, A.; Müller, E.; Habicht, K.; Fritsch, K. Structure, Phase Composition, and Thermoelectric Properties of Yb_xCo₄Sb₁₂ and Their Dependence on Synthesis Method. *ACS Appl. Energy Mater.* **2018**, *1*, 113–122.

- (45) Hohenberg, P.; Kohn, W. Inhomogeneous Electron Gas. *Phys. Rev.* **1964**, *136*, B864–B871.
- (46) Kohn, W.; Sham, L. J. Self-Consistent Equations Including Exchange and Correlation Effects. *Phys. Rev.* **1965**, *140*, A1133–A1138.
- (47) Kresse, G.; Furthmüller, J. Efficiency of ab-initio total energy calculations for metals and semiconductors using a plane-wave basis set. *Comput. Mater. Sci.* **1996**, *6*, 15–50.
- (48) Perdew, J. P.; Burke, K.; Ernzerhof, M. Generalized Gradient Approximation Made Simple. *Phys. Rev. Lett.* **1996**, *77*, 3865–3868.
- (49) Blöchl, P. E. Projector augmented-wave method. *Phys. Rev. B* **1994**, *50*, 17953–17979.
- (50) Kresse, G.; Joubert, D. From ultrasoft pseudopotentials to the projector augmented-wave method. *Phys. Rev. B* **1999**, *59*, 1758–1775.
- (51) Methfessel, M.; Paxton, A. T. High-precision sampling for Brillouin-zone integration in metals. *Phys. Rev. B* **1989**, *40*, 3616–3621.
- (52) Blöchl, P. E.; Jepsen, O.; Andersen, O. K. Improved tetrahedron method for Brillouin-zone integrations. *Phys. Rev. B* **1994**, *49*, 16223–16233.
- (53) Saal, J. E.; Kirklin, S.; Aykol, M.; Meredig, B.; Wolverton, C. Materials Design and Discovery with High-Throughput Density Functional Theory: The Open Quantum Materials Database (OQMD). *JOM* **2013**, *65*, 1501–1509.
- (54) Kirklin, S.; Saal, J. E.; Meredig, B.; Thompson, A.; Doak, J. W.; Aykol, M.; Rühl, S.; Wolverton, C. The Open Quantum Materials Database (OQMD): assessing the accuracy of DFT formation energies. *npj Comput. Mater.* **2015**, *1*, 15010.
- (55) Fontaine, D. D. In *Solid State Physics*; Ehrenreich, H., Turnbull, D., Eds.; Academic Press, 1994; Vol. 47; pp 33–176.
- (56) Zunger, A. In *Statics and Dynamics of Alloy Phase Transformations*; Turchi, P. E. A., Gonis, A., Eds.; NATO ASI Series; Springer US: Boston, MA, 1994; pp 361–419.
- (57) van de Walle, A.; Asta, M.; Ceder, G. The alloy theoretic automated toolkit: A user guide. *Calphad* **2002**, *26*, 539–553.
- (58) Zunger, A.; Wei, S.-H.; Ferreira, L. G.; Bernard, J. E. Special quasirandom structures. *Phys. Rev. Lett.* **1990**, *65*, 353–356.
- (59) Jiang, C.; Wolverton, C.; Sofo, J.; Chen, L.-Q.; Liu, Z.-K. First-principles study of binary bcc alloys using special quasirandom structures. *Phys. Rev. B* **2004**, *69*, 214202.
- (60) Doak, J. W.; Wolverton, C. Coherent and incoherent phase stabilities of thermoelectric rocksalt IV-VI semiconductor alloys. *Phys. Rev. B* **2012**, *86*, 144202.
- (61) Doak, J. W.; Wolverton, C.; Ozoliņš, V. Vibrational contributions to the phase stability of PbS-PbTe alloys. *Phys. Rev. B* **2015**, *92*, 174306.
- (62) Medeiros, P. V. C.; Stafström, S.; Björk, J. Effects of extrinsic and intrinsic perturbations on the electronic structure of graphene: Retaining an effective primitive cell band structure by band unfolding. *Phys. Rev. B* **2014**, *89*, 041407.
- (63) Medeiros, P. V. C.; Tsirkin, S. S.; Stafström, S.; Björk, J. Unfolding spinor wave functions and expectation values of general operators: Introducing the unfolding-density operator. *Phys. Rev. B* **2015**, *91*, 041116.
- (64) Dille, N. R.; Bauer, E. D.; Maple, M. B.; Sales, B. C. Thermoelectric properties of chemically substituted skutterudites $\text{Yb}_y\text{Co}_4\text{Sn}_x\text{Sb}_{12-x}$. *J. Appl. Phys.* **2000**, *88*, 1948–1951.

- (65) Kim, H.; Kaviany, M.; Thomas, J. C.; Van der Ven, A.; Uher, C.; Huang, B. Structural Order-Disorder Transitions and Phonon Conductivity of Partially Filled Skutterudites. *Phys. Rev. Lett.* **2010**, *105*, 265901.
- (66) Shi, X.; Zhang, W.; Chen, L. D.; Yang, J. Filling Fraction Limit for Intrinsic Voids in Crystals: Doping in Skutterudites. *Phys. Rev. Lett.* **2005**, *95*, 185503.
- (67) Mei, Z. G.; Zhang, W.; Chen, L. D.; Yang, J. Filling fraction limits for rare-earth atoms in CoSb₃: An ab initio approach. *Phys. Rev. B* **2006**, *74*, 153202.
- (68) Shi, X.; Zhang, W.; Chen, L. D.; Yang, J.; Uher, C. Theoretical study of the filling fraction limits for impurities in CoSb₃. *Phys. Rev. B* **2007**, *75*, 235208.
- (69) Shi, X.; Zhang, W.; Chen, L. D.; Yang, J.; Uher, C. Thermodynamic analysis of the filling fraction limits for impurities in CoSb₃ based on ab initio calculations. *Acta Mater.* **2008**, *56*, 1733–1740.
- (70) Bauer, E.; Galatanu, A.; Michor, H.; Hilscher, G.; Rogl, P.; Boulet, P.; Noël, H. Physical properties of skutterudites Yb_xM₄Sb₁₂, M = Fe, Co, Rh, Ir. *Eur. Phys. J. B* **2000**, *14*, 483–493.
- (71) Li, H.; Tang, X.; Su, X.; Zhang, Q.; Uher, C. Nanostructured bulk Yb_xCo₄Sb₁₂ with high thermoelectric performance prepared by the rapid solidification method. *J. Phys. D: Appl. Phys.* **2009**, *42*, 145409.
- (72) Liu, H.; Zhao, X.; Zhu, T.; Gu, Y. Thermoelectric properties of Yb_xCo₄Sb₁₂ system. *J. Rare Earths* **2012**, *30*, 456–459.
- (73) Dahal, T.; Jie, Q.; Joshi, G.; Chen, S.; Guo, C.; Lan, Y.; Ren, Z. Thermoelectric property enhancement in Yb-doped n-type skutterudites Yb_xCo₄Sb₁₂. *Acta Mater.* **2014**, *75*, 316–321.
- (74) Nie, G.; Li, W.; Guo, J. Q.; Yamamoto, A.; Kimura, K.; Zhang, X.; Isaacs, E. B.; Dravid, V.; Wolverton, C.; Kanatzidis, M. G.; Priya, S. unpublished.
- (75) He, C.; Daniel, M.; Grossmann, M.; Ristow, O.; Brick, D.; Schubert, M.; Albrecht, M.; Dekorsy, T. Dynamics of coherent acoustic phonons in thin films of CoSb₃ and partially filled Yb_xCo₄Sb₁₂ skutterudites. *Phys. Rev. B* **2014**, *89*, 174303.
- (76) Fedorov, P. P. Third law of thermodynamics as applied to phase diagrams. *Russ. J. Inorg. Chem.* **2010**, *55*, 1722–1739.
- (77) Anthony, L.; Okamoto, J. K.; Fultz, B. Vibrational entropy of ordered and disordered Ni₃Al. *Phys. Rev. Lett.* **1993**, *70*, 1128–1130.
- (78) Ozoliņš, V.; Asta, M. Large Vibrational Effects upon Calculated Phase Boundaries in Al-Sc. *Phys. Rev. Lett.* **2001**, *86*, 448–451.
- (79) Ozoliņš, V.; Sadigh, B.; Asta, M. Effects of vibrational entropy on the Al-Si phase diagram. *J. Phys.: Condens. Matter* **2005**, *17*, 2197–2210.
- (80) Pomrehn, G. S.; Toberer, E. S.; Snyder, G. J.; van de Walle, A. Entropic stabilization and retrograde solubility in Zn₄Sb₃. *Phys. Rev. B* **2011**, *83*, 094106.
- (81) Mandrus, D.; Migliori, A.; Darling, T. W.; Hundley, M. F.; Peterson, E. J.; Thompson, J. D. Electronic transport in lightly doped CoSb₃. *Phys. Rev. B* **1995**, *52*, 4926–4931.
- (82) Rakoto, H.; Respaud, M.; Broto, J. M.; Arushanov, E.; Caillat, T. The valence band parameters of CoSb₃ determined by Shubnikov–de Haas effect. *Physica B* **1999**, *269*, 13–16.
- (83) Singh, D. J.; Pickett, W. E. Skutterudite antimonides: Quasilinear bands and unusual transport. *Phys. Rev. B* **1994**, *50*, 11235–11238.

- (84) Sofo, J. O.; Mahan, G. D. Electronic structure of CoSb₃: A narrow-band-gap semiconductor. *Phys. Rev. B* **1998**, *58*, 15620–15623.
- (85) Perdew, J. P. Density functional theory and the band gap problem. *Int. J. Quantum Chem.* **1985**, *28*, 497–523.
- (86) Khan, B.; Aliabad, H. A. R.; Saifullah.; Jalali-Asadabadi, S.; Khan, I.; Ahmad, I. Electronic band structures of binary skutterudites. *J. Alloys Compd.* **2015**, *647*, 364–369.
- (87) Khan, B.; Aliabad, H. A. R.; Khan, I.; Jalali-Asadabadi, S.; Ahmad, I. Comparative study of thermoelectric properties of Co based filled antimonide skutterudites with and without SOC effect. *Comput. Mater. Sci.* **2017**, *131*, 308–314.
- (88) Wee, D.; Kozinsky, B.; Marzari, N.; Fornari, M. Effects of filling in CoSb₃: Local structure, band gap, and phonons from first principles. *Phys. Rev. B* **2010**, *81*, 045204.
- (89) Hammerschmidt, L.; Quennet, M.; Töpfer, K.; Paulus, B. Low-index surfaces of CoSb₃ skutterudites from first principles. *Surf. Sci.* **2015**, *637-638*, 124–131.
- (90) Pei, Y.; Shi, X.; LaLonde, A.; Wang, H.; Chen, L.; Snyder, G. J. Convergence of electronic bands for high performance bulk thermoelectrics. *Nature* **2011**, *473*, 66–69.
- (91) Liu, W.; Tan, X.; Yin, K.; Liu, H.; Tang, X.; Shi, J.; Zhang, Q.; Uher, C. Convergence of Conduction Bands as a Means of Enhancing Thermoelectric Performance of *n*-Type Mg₂Si_{1-x}Sn_x Solid Solutions. *Phys. Rev. Lett.* **2012**, *108*, 166601.
- (92) Zhao, L. D.; Wu, H. J.; Hao, S. Q.; Wu, C. I.; Zhou, X. Y.; Biswas, K.; He, J. Q.; Hogan, T. P.; Uher, C.; Wolverton, C.; Dravid, V. P.; Kanatzidis, M. G. All-scale hierarchical thermoelectrics: MgTe in PbTe facilitates valence band convergence and suppresses bipolar thermal transport for high performance. *Energy Environ. Sci.* **2013**, *6*, 3346–3355.
- (93) Wang, H.; Gibbs, Z. M.; Takagiwa, Y.; Snyder, G. J. Tuning bands of PbSe for better thermoelectric efficiency. *Energy Environ. Sci.* **2014**, *7*, 804–811.
- (94) Korotaev, P.; Yanilkin, A. The influence of lattice dynamics on the electronic spectrum of CoSb₃ skutterudite. *J. Mater. Chem. C* **2017**, *5*, 10185–10190.